Unusual Spectroscopic and Electrochemical Properties of the 2[4Fe-4S] Ferredoxin of *Thauera aromatica*[†,‡]

Matthias Boll,*[,§] Georg Fuchs,[||] Gareth Tilley,[⊥] Fraser A. Armstrong,[⊥] and David J. Lowe[§]

Institut für Biologie II, Universität Freiburg, Schänzlestrasse 1, D-79104 Freiburg, Germany, Nitrogen Fixation Laboratory, John Innes Centre, Norwich NR4 7UH, U.K., and Department of Inorganic Chemistry, University of Oxford, South Parks Road, Oxford OX1 3QR, U.K.

Received December 6, 1999; Revised Manuscript Received February 3, 2000

ABSTRACT: A reduced ferredoxin serves as the natural electron donor for key enzymes of the anaerobic aromatic metabolism in the denitrifying bacterium *Thauera aromatica*. It contains two [4Fe-4S] clusters and belongs to the *Chromatium vinosum* type of ferredoxins (CvFd) which differ from the "clostridial" type by a six-amino acid insertion between two successive cysteines and a C-terminal α-helical amino acid extension. The electrochemical and electron paramagnetic resonance (EPR) spectroscopic properties of both [4Fe-4S] clusters from *T. aromatica* ferredoxin have been investigated using cyclic voltammetry and multifrequency EPR. Results obtained from cyclic voltammetry revealed the presence of two redox transitions at −431 and −587 mV versus SHE. X-band EPR spectra recorded at potentials where only one cluster was reduced (greater than −500 mV) indicated the presence of a spin mixture of $S = {}^3/_2$ and ${}^5/_2$ spin states of one reduced [4Fe-4S] cluster. No typical $S = {}^1/_2$ EPR signals were observed. At lower potentials (less than −500 mV), the more negative [4Fe-4S] cluster displayed Q-, X-, and S-band EPR spectra at 20 K which were typical of a single $S = {}^1/_2$ low-spin [4Fe-4S] cluster with a g_{av} of 1.94. However, when the temperature was decreased stepwise to 4 K, a magnetic interaction between the two clusters gradually became observable as a temperature-dependent splitting of both the $S = {}^1/_2$ and $S = {}^5/_2$ EPR signals. At potentials where both clusters were reduced, additional low-field EPR signals were observed which can only be assigned to spin states with spins of $> {}^5/_2$. The results that were obtained establish that the common typical amino acid sequence features of CvFd-type ferredoxins determine the unusual electrochemical properties of the [4Fe-4S] clusters. The observation of different spin states in *T. aromatica* ferredoxin is novel among CvFd-type ferredoxins.

Thauera aromatica uses various aromatic compounds as sole sources of cell carbon and energy when grown anaerobically with nitrate as the terminal electron acceptor (*1*−*4*). The Fe−S protein benzoyl-CoA reductase is a key enzyme of anaerobic aromatic metabolism catalyzing the ATP-dependent reductive dearomatization of the central intermediate benzoyl-CoA to a cyclic diene (*5*). Another novel enzyme is the molybdenum cofactor-containing 4-OH-benzoyl-CoA reductase which catalyzes the reductive removal of a phenolic hydroxy group from the aromatic ring (*6*, *7*).

A ferredoxin has recently been purified from *T. aromatica* (TaFd);[1] this has been shown to serve in the reduced state as the electron donor to benzoyl-CoA reductase and 4-OH-benzoyl-CoA reductase (*7*, *8*) (Figure 1). In preliminary biochemical studies, the 9.6 kDa ferredoxin has been shown to contain 7.6 ± 0.6 mol of iron and 7.6 ± 1.0 mol of acid labile sulfur/mol (*8*). The reduction potential of the Fe−S clusters of TaFd was −445 mV (vs SHE) as determined by ultraviolet−visible spectroscopy in the presence of methyl viologen. However, due to uncertainties in the determination of protein and extinction coefficients of reduced and oxidized ferredoxin, it remained unclear whether both Fe−S clusters were completely reduced at this potential (*8*). Amino acid and gene sequence analysis revealed the presence of eight cysteinyl residues with high degrees of similarity to the 2[4Fe-4S] cluster-containing *Chromatium vinosum* type of ferredoxins.

Ferredoxins belonging to the *C. vinosum* type exhibit two special sequence elements which distinguish them clearly from the "clostridial type": a six-amino acid insertion between two cysteines of the typical CxxCxxC···CP se-

[†] This work was supported by grants from the EC BIOTECH program, the Deutsche Forschungsgemeinschaft, the Fonds der Chemischen Industrie, and the EPSRC/BBSRC. Research in Oxford was supported by grants from BBSRC and EPSRC and in Norwich by BBSRC.

[‡] Dedicated to Professor Rudolf Thauer, Marburg, on the occasion of his 60th birthday.

* To whom correspondence should be addressed: Institut für Biologie II, Universität Freiburg, Schänzlestr. 1, D-79104 Freiburg, Germany. Telephone: +49 761 203 2685/2681. Fax: +49 761 203 2626. E-mail: boll@uni-freiburg.de.

[§] John Innes Centre.

[||] Universität Freiburg.

[⊥] University of Oxford.

[1] Abbreviations: TaFd, *T. aromatica* ferredoxin; CvFd, *C. vinosum* ferredoxin; AvFdIII, *A. vinelandii* ferredoxin III; CpFd, *Clostridium pasteurianum* ferredoxin; SHE, standard hydrogen electrode; HEPES, *N*-(2-hydroxyethyl)piperazine-*N*′-2-ethanesulfonic acid; TEA, triethanolamine; MES, 2-(*N*-morpholino)ethanesulfonic acid; TAPS, *N*-tris-(hydroxymethyl)methyl-3-aminopropanesulfonic acid.

10.1021/bi9927890 CCC: $19.00
Published on Web 03/31/2000

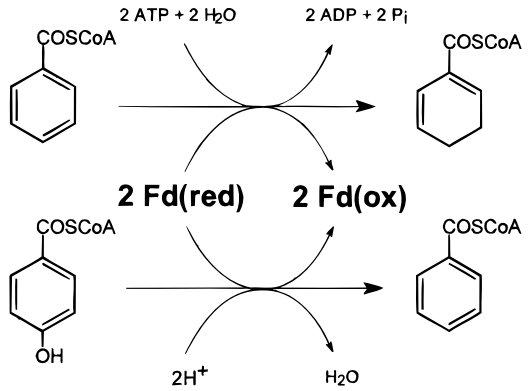

FIGURE 1: Key enzymatic reactions of the anaerobic aromatic metabolism of *T. aromatica* involving reduced ferredoxin as in vivo electron donor. Since this work shows that only one cluster of TaFd is likely to be reduced under physiological conditions, a stoichiometry of 2 reduced ferredoxins/benzoyl-CoA is assumed.

quence motif (where x is a variable amino acid) which represents the binding site of the N-terminal [4Fe-4S] cluster and a long N-terminal amino acid extension (*9*). Two ferredoxins of this type, *C. vinosum* ferredoxin (CvFd) (*10*−*12*) and *Azotobacter vinelandii* ferredoxin III (AvFdIII) (*13*), have been investigated further by electrochemical and spectroscopic means. The [4Fe-4S] clusters of these ferredoxins exhibit unusual electrochemical properties. In contrast to clostridial-type ferredoxins, which have two [4Fe-4S] clusters with essentially identical reduction potentials of approximately −400 mV (vs SHE), the reduction potentials of CvFd-type [4Fe-4S] clusters are more negative and differ widely (−460 and −655 mV in CvFd and −486 and −644 mV in AvFdIII) (*11*, *13*).

In this work, we report on the characterization of the 4Fe-4S clusters of *T. aromatica* ferredoxin by multifrequency EPR spectroscopy at defined electrode potentials and by cyclic voltammetric studies. The results reveal some unusual spectroscopic, magnetic, and electrochemical properties. As shown for the two ferredoxins of the *C. vinosum* type studied so far, the [4Fe-4S] clusters differ widely in their reduction potentials. But uniquely for 2[4Fe-4S] ferredoxins, the spin states of both clusters are also different: one where $S = {}^1/_2$ and the other where $S = {}^3/_2$ and ${}^5/_2$. Moreover, we detected a magnetic interaction between two clusters with different spin states. This interaction is shown to exhibit an unusual temperature dependence. In contrast to other electrochemically and spectroscopically investigated ferredoxins of the CvFd type, the function of TaFd as the electron donor for benzoyl-CoA reductase is known.

EXPERIMENTAL PROCEDURES

Growth of Bacterial Cells. T. aromatica was grown anoxically at 28 °C in a mineral salt medium. 4-Hydroxybenzoate and nitrate in a molar ratio of 1:3.5 served as sole sources of energy and cell carbon. Continuous feeding of the substrates, cell harvesting, storage, and preparation of cell extracts were carried out as described previously (*3*).

Protein Purification and Sample Storage. Purification of ferredoxin was performed under strictly anaerobic conditions in a glovebox under a N_2/H_2 (95:5, by volume) atmosphere as described previously (*8*). The procedure included anion exchange chromatography on DEAE-Sepharose and Q-Sepharose as well as gel filtration using Sephadex G-75. Concentration of the protein samples was achieved by binding them to a Q-Sepharose column [equilibrated with 20 mM TEA (pH 7.8)] followed by elution at a high salt concentration (800 mM KCl step gradient in the same buffer). Further concentration to 1−2 mM was obtained by centrifugation (8000*g*) in Microsep microconcentrators (exclusion limit of 10 kDa). Purified ferredoxin (80 mg) was obtained from 200 g of cells (wet mass). Concentrated protein samples were stored anaerobically at −80 °C for several months.

Redox Titration of Ferredoxin. Dye-mediated redox titrations of ferredoxin were performed in a Miller-Howe anaerobic glovebox under a nitrogen atmosphere (<1 ppm O_2). The ferredoxin/mediator mixture (2.5 mL) was in 20 mM TEA/KOH (pH 7.8) containing 800 mM KCl. For the removal of any redox active substance (e.g., dithionite), and for buffer exchange, the ferredoxin was passed through a Biogel P-6 gel filtration column (volume of 5 mL, diameter of 1 cm) which had been equilibrated with either a 100 mM potassium phosphate buffer with 500 mM KCl (pH 7.0−8.0) or a 100 mM Tris-HCl buffer (pH 8.0−10.0) containing 500 mM KCl. The final concentration of ferredoxin was 300−850 μM. The mediator solution consisted of methyl and benzyl viologens, neutral red, safranin O, phenosafranin, anthraquinone 2-sulfonate, 2-hydroxy-1,4-naphthoquinone, indigo disulfonate, resorufin, methylene blue, phenazine methosulfate, and *N*′,*N*′,*N*′,*N*′-tetramethyl-*p*-phenylenediamine at final concentrations of 40 μM each. The redox potential was adjusted with 10−100 mM sodium dithionite and potassium ferricyanide prepared freshly and anaerobically in the same buffer as the ferredoxin. Potentials reported in this paper were corrected to the SHE scale by using *E*(calomel electrode) = 243 mV versus SHE for the saturated calomel electrode at 22 °C (*14*). Mediator/ferredoxin mixtures with a stable potential could be obtained over the range of −610 to 100 mV. Stabilization (drift < 1 mV/min) of the potentials usually required 1−5 min under continuous stirring. Samples with defined redox potentials were immediately frozen anaerobically in EPR tubes and stored in liquid nitrogen. Redox titrations were normally performed in the oxidative direction, but as a control for reversibility, some samples were prepared by re-reduction with dithionite.

EPR Spectroscopy. All samples were prepared and frozen in EPR tubes under a 100% nitrogen atmosphere in a glovebox (<1 ppm O_2). The concentration of ferredoxin was usually 0.3−1 mM. Prior to reduction, ferredoxin was passed over a Bio-Rad P-6 column as described above. Ferredoxin samples were reduced either by sodium dithionite or by photoreduction. The latter reduction was performed using 25−40 μM deazaflavin in 100 mM Tris buffer (pH 8.0), illuminated in an airtight sealed glass tube (diameter of 1 cm) for 15 min with white light (250 W halogen bulb) focused on each side of the tube (distance of approximately 1−2 cm).

X-band EPR spectra were recorded on an updated Bruker 200D-SRC spectrometer. Low-temperature measurements were made using an Oxford Instruments ESR 900 cryostat modified to take sample tubes with internal diameters of up to 4 mm. Recording conditions are described in the legends of the individual figures. Spin concentrations of ground-state-transition EPR signals were determined by comparison with those of a 1 mM copper sulfate sample in 11 mM sodium

EDTA. Spin concentrations of excited-state transitions were corrected for the temperature dependence of the signal intensity, which allowed the axial zero-field parameter *D* to be determined. Rhombicity (*E*/*D* values) were estimated from the line shape and from the *g* values of other accompanying EPR signals. These parameters allowed the population of the excited-state transitions to be estimated. Q-band and S-band EPR spectra were recorded on a Bruker ESP300-E spectrometer. The resonator at S-band was model ER4118SPT-N1 and at Q-band model ER5106QT. Cooling to 4.2 K was achieved with an Oxford Instruments CF9350 cryostat, and microwave frequencies were measured using an EIP model 588C microwave pulse counter.

Electrochemistry. An AutoLab electrochemical analyzer (Eco Chemie, Utrecht, The Netherlands) was used to record DC voltammograms. The three-electrode configuration featuring all-glass cells has been described previously (*15*). The sample compartment (typically holding 500 μL) was maintained at 0 °C to optimize stability. All potential values are given with reference to SHE. The saturated calomel electrode was held at 22 °C. Reduction potentials from cyclic voltammetry were calculated as the average of the anodic and the cathodic peak potentials, $E^{\circ\prime} = {}^1/_2(E_{pa} + E_{pc})$. The pyrolytic graphite electrode "edge" (PGE) electrode (surface area of typically 0.18 cm^2) was polished before each experiment with an aqueous alumina slurry (1.0 μM, Buehler Micropolish) and then sonicated extensively to remove traces of Al_2O_3. All experiments were carried out under anaerobic conditions in an anaerobic box with an inert atmosphere of N_2 (<1.0 ppm O_2).

For bulk solution electrochemistry, a 100 μM protein solution in a 60 mM mixer buffer (15 mM HEPES, 15 mM MES, 15 mM TAPS, and 15 mM sodium acetate) with a 0.1 M NaCl supporting electrolyte and 4 mM coadsorbate neomycin was used. For protein film experiments, a cell solution comprising 60 mM mixer buffer, 0.1 M NaCl, and 1.8 mg mL^{-1} of coadsorbate polymyxin, at three different pHs, was employed. A 100 μM protein solution in 60 mM mixer buffer, 0.1 M NaCl, and 4 mg mL^{-1} polymyxin at pH 6.5 was used to coat the electrode.

RESULTS

Electrochemistry. To characterize the redox properties of TaFd, direct electrochemical experiments were performed. Figure 2 shows data obtained using cyclic voltammetry on the bulk solution and with a protein film. Bulk solution voltammetry at pH 7.0 (0 °C) revealed two well-defined reversible couples, A and B, with reduction potentials of −431 and −587 mV, respectively. Corresponding peak separations at 5 mV s^{-1} were 54 mV, and plots of peak currents versus (scan rate)$^{1/2}$ were linear up to 10 mV s^{-1}, as expected for a reversible diffusion-controlled electrode reaction at this temperature (*14*). Film voltammetry also showed two reversible one-electron signals, A′ and B′, at −427 and −575 mV, respectively (pH 6.8 and 0 °C). These two signals in the entire experiment are assigned to the two [4Fe-4S]$^{2+/1+}$ clusters. In accordance with the nomenclature used for AvFdIII (*11*), we refer to the cluster with the more negative reduction potential (ligated by the first three N-terminal and by the C-terminal cysteinyl residues in CvFd) as cluster B and the other as cluster A. Note that for the

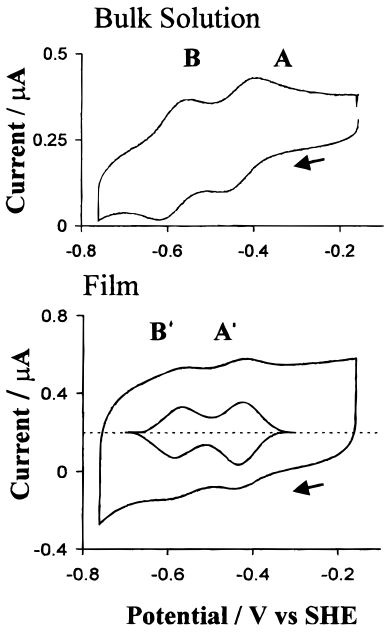

FIGURE 2: Cyclic voltammetry of TaFd. (Top) Bulk solution voltammetry of 100 μM TaFd in 60 mM mixed buffer, 0.1 M NaCl, and 4 mM neomycin at 0 °C and pH 7.0, with a scan rate of 5 mV s^{-1}. (Bottom) Film voltammetry measured in 60 mM mixed buffer, 0.1 M NaCl, and 1.8 mg mL^{-1} polymyxin at 0 °C and pH 6.8, with a scan rate of 20 mV s^{-1}. The background-corrected voltammogram is shown in the center.

[4Fe-4S] clusters in CvFd a different nomenclature is used: cluster A in FdIII and TaFd refers to cluster II in CvFd, and cluster B refers to cluster I. The signals have approximately equal areas in each type of voltammetry (areas for film voltammograms measured after baseline subtraction). The shapes and half-height widths of signals in the film voltammograms, 94 mV for A′ and 108 mV for B′ (each at 20 mV s^{-1}; theoretical value of 83 mV at 0 °C for a one-electron process), are consistent with single redox transitions of species bound in a reasonably homogeneous manner on the electrode surface. Film voltammetry experiments at pH 5.4, 6.8, and 8.3 showed little change in the reduction potential of signal B′. The reduction potential of A′ is similar at pH 5.4 and 6.8 but decreased by 21 mV to −448 mV between pH 6.8 and 8.3.

EPR Redox Titration Studies. X-band EPR redox titration studies were performed both to determine the EPR spectroscopic characteristics of TaFd and to confirm the electrochemical results obtained by cyclic voltammetry. A major goal was to elucidate whether the typical cluster ligation of CvFd-type ferredoxins results both in alterations of the reduction potentials of the redox clusters and in unusual spectroscopic properties that differ from those of the well-described $S = {}^1/_2$ state of reduced CpFd-type [4Fe-4S]$^{1+}$ clusters.

In the ferricyanide-oxidized state, both [4Fe-4S] clusters of TaFd were diamagnetic (no EPR signal), indicating that no high-potential [4Fe-4S]$^{2+/3+}$ redox transition occurred at potentials up to 250 mV. The absence of a signal of a [3Fe-4S]$^{0/1+}$ cluster at positive potentials clearly excluded the presence of a [7Fe-8S] ferredoxin as well as artificial cluster degradation from [4Fe-4S] to [3Fe-4S].

Reduction of TaFd by dithionite at pH 8.5 enabled us to poise potentials as low as −614 mV. From the results

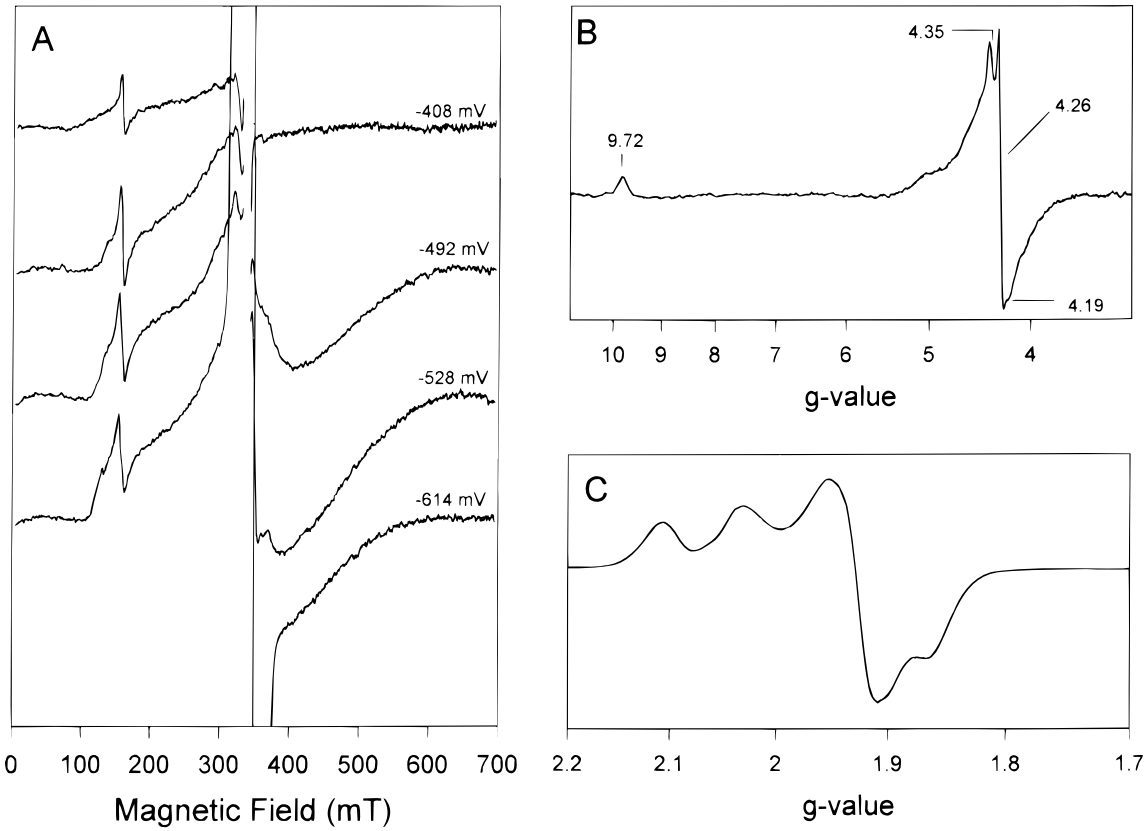

FIGURE 3: Representative EPR spectra obtained in redox titration experiments with TaFd. The samples (0.3−1 mM) were prepared anaerobically in 100 mM potassium phosphate buffer with 500 mM KCl at pH 7.5 (for potentials above −500 mV) or in 100 mM Tris-HCl with 500 mM KCl at pH 8.5 (for potentials below −500 mV). A redox mediator mixture (final concentration of 0.04 mM) was added to the sample solution. Reduction of the samples was performed with sodium dithionite and oxidation with 2,6-dichlorophenolindophenol or ferricyanide (with a 10−100 mM anaerobic stock solution). A calomel electrode in saturated KCl served as the reference electrode. (A) Full-scale EPR spectra. For better presentation, the radical EPR signals from the redox mediators at 340 mT are omitted. Note that the additional large off-scale signal at −614 mV in the 340 mT region is not only due to a radical and is shown separately on an appropriate scale in panel C. EPR conditions were as follows: microwave frequency, 9.4244 GHz; microwave power, 20 mW; modulation amplitude, 1.16 mT; modulation frequency, 100 kHz; and temperature, 4.2 K. (B) Low-field EPR spectrum of TaFd at −493 mV. EPR conditions were as described for panel A but at a microwave power of 40 mW. The numbers on the graph are g values. Note that only cluster A is reduced at this potential. (C) EPR spectrum of the $g = 2$ region of TaFd at −614 mV. EPR conditions were as described for panel A but at a microwave power of 2 mW. Note that cluster A is 100% and cluster B 80% reduced at this redox potential.

obtained from cyclic voltammetry, the complete reduction of cluster A and at least partial reduction of cluster B should be possible in this redox span. Representative EPR spectra recorded at different reduction levels are presented in Figure 3. It shows EPR spectra of TaFd poised at four different potentials where the individual clusters were 10−20% and 80−90% reduced, respectively. At −408 mV, cluster A is only 20% reduced whereas reduction of cluster B is negligible. At this potential, EPR signals were detectable in the $g = 4.3$ and 2 regions (Figure 3A). Both signals became more intense at −492 mV when cluster A was 90% reduced (cluster B being <5% reduced). The signal at $g = 4.3$ is shown in Figure 3B in more detail. From the line shape and temperature dependence of the signal intensity (optimum at 25 K), we assign it to the first excited-state transition of an $S = {}^5/_2$ high-spin system with $g_z = 4.35$, $g_y = 4.26$, and $g_x = 4.19$. An E/D value of 0.31 was estimated from the line shape. This high rhombicity was confirmed by the expected concomitant rise of a second signal at $g = 9.7$. The intensity of this second signal was inversely proportional to temperature according to Curie's law. It was only detectable at temperatures below 10 K and at high microwave power (>20 mW) and impossible to saturate with our equipment down to 4 K with a maximal microwave power of 200 mW. At E/D values of >0.3, a signal at $g = 9.7$ is expected from the ground-state transition of an $S = {}^5/_2$ high-spin system. The quantitation of the EPR signal with $g_{av} = 4.3$ required the evaluation of the energy separation between the two Kramer doublets ($\pm{}^5/_2$). This was estimated from the slope of a plot of temperature versus signal intensity (maximal peak intensity was at 25 K, not shown) which enabled us to determine the axial zero-splitting parameter $D = 4-5$ cm^{-1}. With this D value, the population of the $S = \pm{}^3/_2$ Kramer doublet (first excited sublevel of an $S = {}^5/_2$ high-spin system) was approximately 40% at 25 K, which gave a total number of 0.6−0.7 spin per molecule. Note that integration of this signal was difficult since it overlapped a second very broad EPR signal which will be described below. We therefore estimate that the accuracy of this spin integration was not better than 20%.

EPR signals at $g = 4.3$ often arise from adventitious Fe^{3+}. However, two reasons clearly argue against this possibility in this case and provide evidence that this signal is indeed characteristic for cluster A of TaFd. (a) In the fully oxidized state of TaFd, at potentials above −350 mV, only a very small signal at $g = 4.3$ was observed. The intensity of this signal increased at potentials below −400 mV, corresponding to the observed $E^{\circ\prime}$ value of −435 mV for cluster A as

determined by cyclic voltammetry (Figure 2). In the case of adventitious Fe^{3+}, a decrease in the intensity of the EPR signal due to reduction to diamagnetic Fe^{2+} would be expected. (b) The slightly rhombic line shape and the presence of three clearly distinguishable g values are atypical for free, tetrahedrally coordinated, Fe^{3+} which normally displays an axial signal at $g = 4.3$.

The second EPR signal observed at potentials above −500 mV displays a very broad line shape spanning the interval from 150 to 600 mT (Figure 3A). It was only detectable at low temperatures (<10 K) and high microwave powers (>10 mW), indicating an EPR signal of a ground-state transition. Additionally, in the low-field region of this broad EPR signal, a shoulder at $g \sim 5$ could be distinguished from the much sharper features of the $g = {}^5/_2$ signal described above with $g_{av} = 4.3$, by decreasing the temperature and increasing the microwave power. EPR spectra of [4Fe-4S] clusters with $S = {}^1/_2$ are typically relatively sharp, with a rhombic line shape and $g_{av} = 1.94$, and are normally less than 100 mT wide at X-band frequencies. No such feature was observed at potentials where only cluster A was reduced (Figure 3A). However, the combination of a very broad derivative-shaped signal around $g = 2$ and a poorly resolved absorption signal at $g = 4-5$ is typical for the ground-state transition of an $S = {}^3/_2$ high-spin system ($M_s = \pm{}^1/_2$). The quantification of such anisotropic EPR signals is extremely difficult due to their broad line shape and, as in our case, other overlapping EPR signals. Moreover, we cannot completely rule out a partial contribution of the excited-state sublevel ($\pm{}^3/_2$) of the $S = {}^3/_2$ high-spin system, since for high E/D values the corresponding g values are similar to those of the ground-state transition. Therefore, it was not possible to determine absolute but only relative intensities at different redox potentials. As shown for the $g_{av} = 4.3$ signal assigned to the $S = {}^5/_2$ system, the magnitudes of the $S = {}^3/_2$ EPR signals also increased continuously with the reduction of cluster A (Figures 3A and 4). Therefore, we conclude that cluster A exhibits EPR properties of an $S = {}^3/_2$ and ${}^5/_2$ high-spin mixture.

In Figure 4, the relative spin concentrations of the $S = {}^3/_2$ and ${}^5/_2$ signals are plotted versus the electrode potential. At potentials between −400 and −435 mV, the spin concentration of the $S = {}^5/_2$ signals fitted well to a Nernst curve with an $E^{\circ\prime}$ of −435 mV and an n of 1 up to 0.6 spin/molecule. However, a further decrease in the potential did not result in a change of spin concentration in the $S = {}^5/_2$ EPR signal. This could be explained either by an inaccuracy in the determination of the absolute spin concentration or by redox potential-dependent changes of the spin state of the cluster. In contrast, the relative intensities of the $S = {}^3/_2$ high-spin signal increased continuously in a range from −400 to −540 mV. For this signal, the half-maximal intensity was at −475 mV which does not fit with the value determined by cyclic voltammetry for cluster A of $E^{\circ\prime} = -431$ mV. However, since both the $S = {}^5/_2$ and ${}^3/_2$ spin systems are considered to contribute to the redox transition at −431 mV observed in cyclic voltammetric experiments, the sum of both high-spin systems was compared with an appropriate Nernst curve. With an $S = {}^5/_2$ and ${}^3/_2$ spin ratio of 3:1, the sum of both spins concentrations would fit to a Nernst curve with an $E^{\circ\prime}$ of −435 mV and an n of 1 as shown in Figure 4. However, we emphasize that since it was not possible to determine the absolute values for the $S = {}^3/_2$ species, the fit to the Nernst curve is presented for demonstrative purposes only. Note that independent of the absolute value for the $S = {}^3/_2$ spin concentration, the ratio of $S = {}^3/_2$ to ${}^5/_2$ intensities was not constant between −400 and −520 mV (Figure 4).

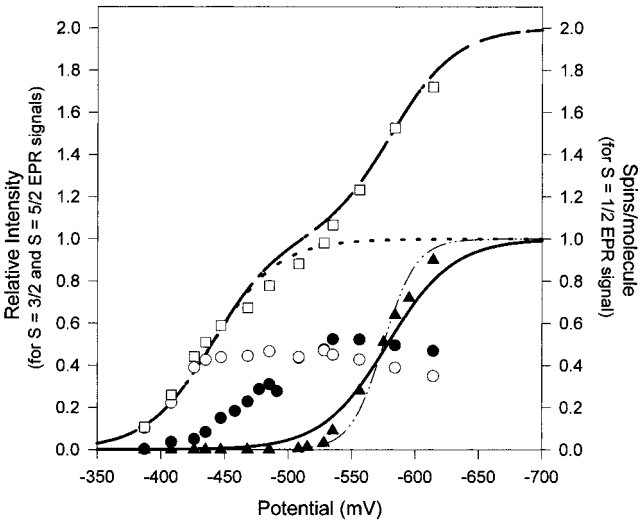

FIGURE 4: Relative ($S = {}^3/_2$ and ${}^5/_2$) and total ($S = {}^1/_2$) spin concentrations of the individual EPR signals during a redox titration of TaFd. The quantification of the $S = {}^1/_2$ and ${}^5/_2$ EPR signals is described in the Results. Note that the absolute spin concentration of the $S = {}^3/_2$ signal could not be determined. Therefore, the relative intensities were measured by the amplitude of the signals at 270 and 420 mT and compared with the corresponding $S = {}^5/_2$ spin concentrations. For better presentation, the sum of all signals was determined by using an $S = {}^5/_2$ to $S = {}^3/_2$ spin concentration ratio of 3:1: (▲) $S = {}^1/_2$ EPR signal with $g_{av} \sim 1.94$ as shown in Figure 3C, (○) $S = {}^5/_2$ EPR signal with $g_{av} \sim 4.3$ as shown in Figure 3A, (●) broad EPR signal with $g_{av} \sim 2$, assigned to an $S = {}^3/_2$ system as shown in Figure 3A, and (□) total amount of spins as calculated by addition of the spin concentrations of the three signals described above. (···) Nernst curve for $E^{\circ\prime} = -435$ mV and $n = 1$. (—) Nernst curve for $E^{\circ\prime} = -575$ mV and $n = 1$ and 2. (- - -) Sum of both curves.

Cyclic voltammetric studies indicated that at potentials below −500 mV, cluster B should become reduced since its $E^{\circ\prime}$ is −587 mV. As shown in Figures 3A and 4, the EPR signals of the $S = {}^3/_2$ and ${}^5/_2$ systems, both assigned to cluster A, did not change significantly in their spin concentration, indicating that reduction of cluster A was complete as expected from the cyclic voltammetric results. Below −500 mV, novel EPR features arose in the $g = 2$ region. These had properties of the $S = {}^1/_2$ EPR signal (Figure 3C). However, they were not typical of a single, isolated [4Fe-4S] cluster; they appeared more like the signal of one [4Fe-4S] cluster coupled to a second spin. Spin integration was 0.92 spin/molecule at −614 mV. Since at this potential cluster B is only ∼85% reduced, the spin concentration of this EPR signal was extrapolated to a value of ∼1.15 spins/molecule for fully reduced cluster B. In Figure 4, the spin concentration of the $S = {}^1/_2$ EPR signal is plotted against the redox potential. It fitted best to a Nernst curve with an $E^{\circ\prime}$ of −575 mV which was close to the corresponding value obtained by cyclic voltammetry. The slope of the curve did not clearly indicate the number of electrons transferred since n was between 1 and 2. However, because of a small decrease in the intensities of the high-spin signals in this range of redox potentials, when the sum of the concentrations of all three EPR detectable spin states was plotted against

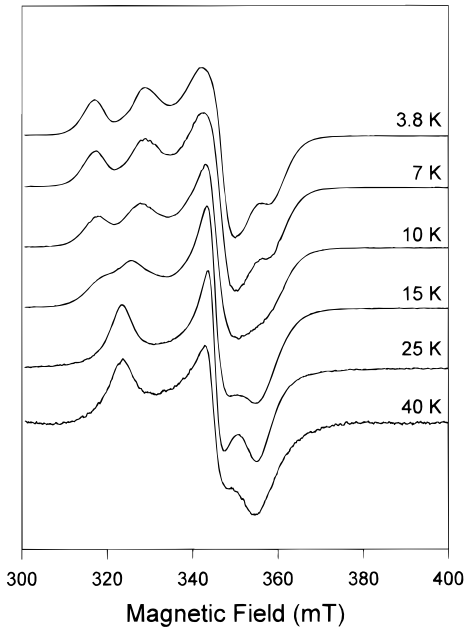

FIGURE 5: Effect of temperature on the $S = {}^1/_2$ EPR signals of photoreduced TaFd (600 μM). The intensities of the EPR signals are corrected for temperature according to Curie's law. Reduction of the samples was by addition of 40 μM deazaflavin (and 0.02 M Tris) and illumination for 15 min with white light. The sample was in 100 mM TEA-HCl and 500 mM KCl at pH 7.5. EPR conditions were as follows: microwave frequency, 9.442 GHz; microwave power, 2 mW; modulation amplitude, 0.36 mT; and modulation frequency, 100 kHz. Note that the measured spin concentration was 1.15 ± 0.1 spins/molecule and did not vary with temperature.

the redox potential, the curve did correspond to two distinct redox transitions with an *n* of 1 (Figure 4).

Temperature Dependence of the $S = {}^1/_2$ EPR Signal. The $S = {}^1/_2$ EPR signal was further characterized by studying the temperature dependence of its line shape and intensity (Figure 5). Surprisingly, the line shape of the EPR signal changed markedly in a range from 7 to 20 K. At temperatures of ≤7 K, the line shape was characteristic of a [4Fe-4S] cluster interacting with a second spin, whereas at temperatures above 20 K, the line shape was typical of a single, isolated [4Fe-4S] cluster. The transition from the "split" line shape to the "nonsplit" line shape occurred continuously between 7 and 20 K, with a "half-split" state (split/nonsplit ratio ∼ 1) at ∼12 K as estimated from the temperature-dependent changes of the signal amplitude at $g = 2.11$ (coupled form) and $g = 2.07$ (uncoupled form). The spin concentration remained constant from 4 to 30 K at 1.1−1.2 spins/molecule. At higher temperatures, relaxation broadening effects made an accurate quantitation impossible. At 3.8 K and a microwave power of 2 mW, no significant saturation of the EPR signal occurred; saturation started at 20 mW at 7 K. We also checked whether these temperature-dependent changes were affected by electrode potential and, consequently, by the degree of reduction of cluster B as described for CvFd (*11*). In Figure 6, EPR spectra recorded at 4 and 20 K at −535 mV (cluster B is ∼10% reduced) and −614 mV (cluster B is 85% reduced) are presented. This clearly shows that the line shape of the $S = {}^1/_2$ EPR spectrum was not affected by the level of reduction of cluster B at either 4 or 20 K.

Multifrequency EPR Spectroscopy of the $S = {}^1/_2$ Signal. Multifrequency EPR spectroscopy was used to clarify further

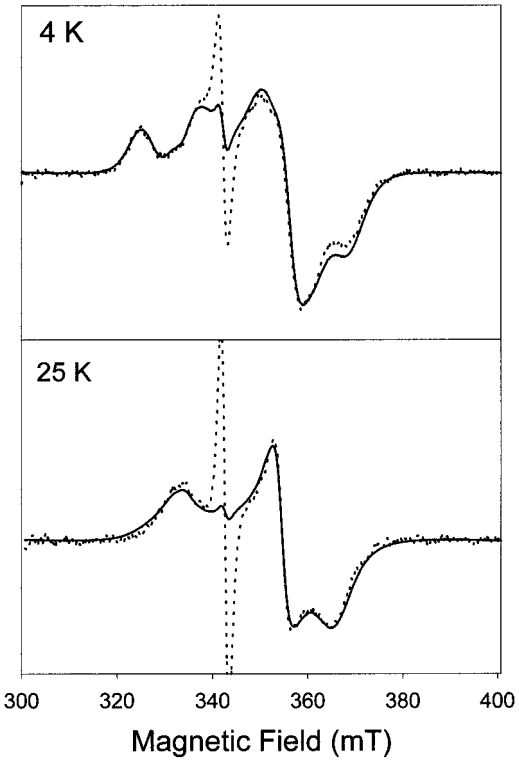

FIGURE 6: Effect of temperature and redox potential on the $S = {}^1/_2$ EPR signal of TaFd. TaFd samples, 450 μM in Tris-HCl buffer at pH 8.3, were prepared as described in the legend of Figure 3. EPR spectra recorded at (—) −614 and (•••) −535 mV. The intensity of the −535 mV spectrum was multiplied by a factor of 11.5. The isotropic signal at $g = 2.005$ is due to viologen radical signals present in the redox mediator cocktail. EPR conditions were as described in the legend of Figure 5.

the unusual temperature-dependent switch from interacting to noninteracting $S = {}^1/_2$ EPR signals. Figure 7 shows the EPR spectra recorded at three different microwave frequencies at 4 and 20 K. The temperature-dependent changes in the line shape of the $S = {}^1/_2$ EPR signals as detected at X-band frequencies were also observable with S-band and Q-band EPR spectroscopy. Multifrequency EPR studies confirmed the assumption that the 20 K EPR spectrum, which was typical for a single, isolated cluster, was split at lower temperatures in a manner consistent with a magnetic interaction with a second cluster. In the *z*-direction (lowest-field features), a splitting constant, *Az*, of 12 mT was determined which was independent of the magnetic field (Figure 7). The splitting constants in *x*- and *y*-directions were more difficult to determine; a rough estimation for the X-band sample suggested *Ay* ∼ 3 mT and *Ax* ∼ 6 mT.

Temperature Dependence of the $S = {}^5/_2$ Signals. From the results reported so far in this work, TaFd consists of two 4Fe-4S clusters of which the one with the less negative reduction potential is a mixture of $S = {}^3/_2$ and ${}^5/_2$ high-spin systems and the one with the more negative reduction potential is an $S = {}^1/_2$ system with a temperature-dependent interaction with a second cluster. We therefore checked the effect of temperature on the line shape of the $S = {}^5/_2$ signal at redox potentials when both clusters were almost completely reduced. Figure 8 shows the temperature dependence of the low-field EPR spectra of TaFd at −614 mV. The $g_{av} = 4.3$ signal, which was assigned to the first excited-state transition of an $S = {}^5/_2$ high-spin system, displays a more

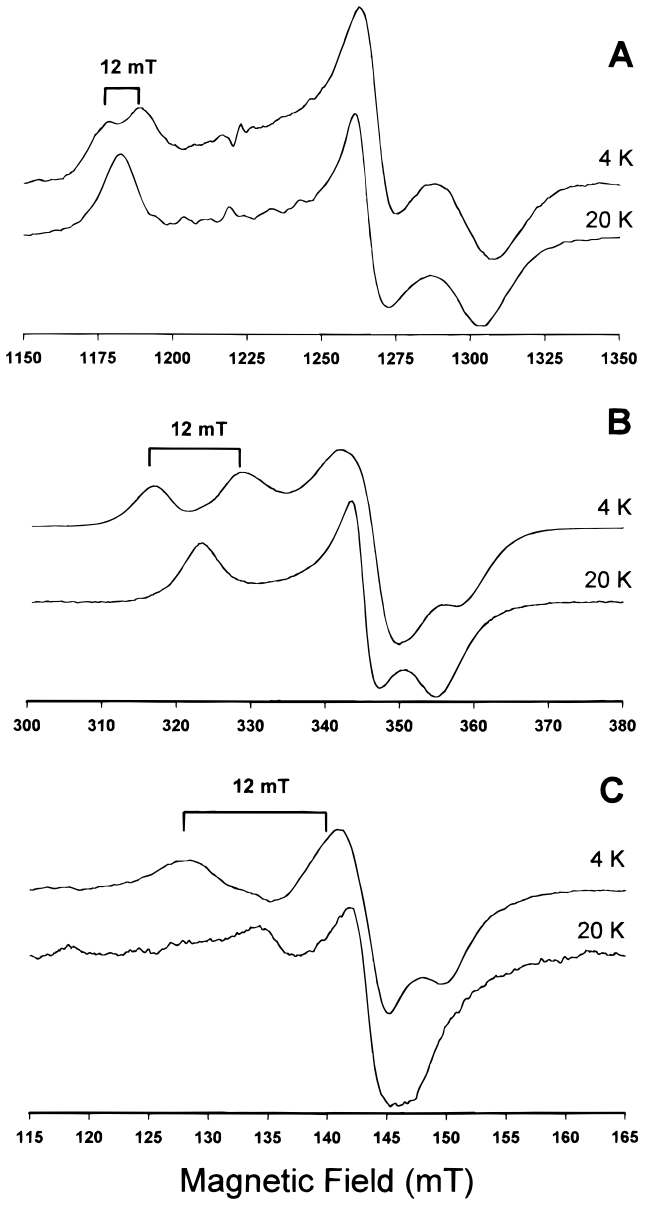

FIGURE 7: Multifrequency EPR spectroscopy with TaFd at different temperatures. The protein concentration was 240−520 μM in 100 mM TEA-HCl (pH 7.5) and 500 mM KCl. Protein was reduced by dithionite. (A) Q-band EPR spectra. EPR conditions were as follows: microwave frequency, 33.875 GHz; microwave power, 0.09 mW (4 K spectrum) and 12.2 mW (20 K spectrum); modulation amplitude, 1.0 mT; and modulation frequency, 100 kHz. Note that the structure between 1200 and 1250 mT is caused by minor ($\ll$1%) impurities of Mn^{2+}. (B) X-band EPR spectra. EPR conditions were as follows: microwave frequency, 9.442 GHz; microwave power, 2 mW (4 K spectrum) or 20 mW (20 K spectrum); modulation amplitude, 0.37 mT; and modulation frequency, 100 kHz. (C) S-Band spectra. EPR conditions were as follows: microwave frequency, 3.874 GHz; microwave power, 20 mW (4 K spectrum) or 50 mW (20 K spectrum); modulation amplitude, 1.995 mT; and modulation frequency, 100 kHz. All spectra were corrected for power, temperature, and modulation amplitude.

axial line shape at temperatures above 25 K. When the temperature was decreased, a change in the line shape could be observed in the range between 4 and 25 K. In the same way as for the $S = {}^1/_2$ signals of cluster B, the $S = {}^5/_2$ EPR signal of cluster A showed a temperature-dependent switch from a nonsplit to a split form, presumably due to the same temperature-dependent magnetic interaction. To demonstrate

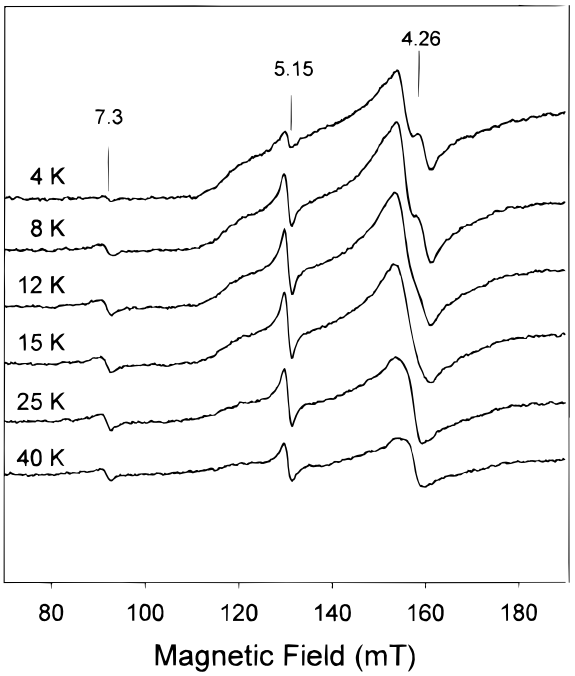

FIGURE 8: Effect of temperature on the low-field EPR signal of reduced TaFd. The sample (350 μM) was in 100 mM Tris-HCl and 500 mM KCl (pH 8.5) and poised to a redox potential of −614 mV. EPR conditions were as follows: microwave frequency, 9.442 GHz; microwave power, 2 mW; modulation amplitude, 0.37 mT; and modulation frequency, 100 kHz.

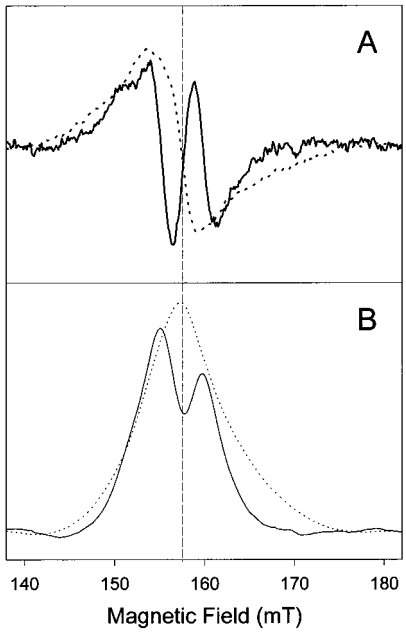

FIGURE 9: Temperature-dependent splitting of the $g = 4.3$ EPR signal of TaFd. Sample and EPR conditions were as described in the legend of Figure 8. (A) EPR first-derivative spectrum recorded at 40 K (···), and difference spectrum between the EPR spectra recorded at 4 and 40 K in Figure 8 (—). (B) EPR absorption spectra of the spectra in panel A. EPR conditions were as described in the legend of Figure 8.

this more clearly, in Figure 9 the derivative (Figure 9A) and integrated (Figure 9B) spectra recorded at 40 K are compared with the difference between spectra recorded at 4 and 40 K. At 40 K, the line shape is not split, whereas the difference spectrum clearly shows the splitting of this peak into two subpeaks (Figure 9B). The splitting was ~3 mT. At 10−15 K, the clusters were 50% uncoupled, consistent with the

Table 1: Amino Acid Sequence Alignment of the Cluster Ligation Region between CvFd-Type and CpFd Ferredoxins and the Reduction Potentials of the Corresponding [4Fe-4S] Clusters

Ferredoxin	Reference	Amino acid binding motif	Reduction potential [4Fe-4S] I**	Reduction potential [4Fe-4S] II**
		I* I* I* II* II*II* II* I*		
TaFd	(5)	.....D-CTACDACVEECPN.....KCSECVGAFDEPQCRLVCPA.....	-587 mV	-431 mV
CvFd	(11)	.....E-CINCDVCEPECPN.....LCTECVGHYETSQCVEVCPV.....	-660 mV	-460 mV
AvFdIII	(13)	.....D-CINCDVCEPECPN.....LCTECVGHYDEPQCQQVCPV.....	-644 mV	-486 mV
CpFd	(18,19)	.....DSCVSCGACASECPV.....TCIDC------GNCANVCPV.....	-400 mV	-400 mV

*Cysteines involved in ligation of cluster I and cluster II. In CvFd cluster I is coordinated by C-8, C-11,C-14 and C-54; cluster II is coordinated by C-18, C-38,C-41 and C-49.
** versus SHE.

corresponding value of 12 K determined for the $S = {}^1/_2$ system. These results indicate that cluster B with $S = {}^1/_2$ interacts with cluster A with $S = {}^5/_2$ and ${}^3/_2$ but that this can only be observed at very low temperatures. It is interesting to note that the weak $g = 9.7$ signal, observed at -500 mV, and assigned to the ground-state transition of the $S = {}^5/_2$ system disappeared upon reduction of cluster B. We suggest that the magnetic interaction between the two clusters should also split the $g = 9.7$ signal but that in contrast to the strong, sharp signal at $g_{av} = 4.3$, this signal is too weak to be observed when it is split due to magnetic interaction with cluster B. Since cluster A is a spin mixture of $S = {}^5/_2$ and ${}^3/_2$ species, and since the spin concentration of the $S = {}^1/_2$ EPR signal is approximately 1 per molecule, we also expected an interaction of the $S = {}^3/_2$ system with the $S = {}^1/_2$ system. However, as described above, the $S = {}^3/_2$ EPR signal is very broad and featureless, making it impossible to detect such interactions.

At very low potentials, when both clusters were reduced, additional low-field EPR signals with $g = 5.15$ and 7.3 were detected. The intensities of both signals decreased at temperatures below 20 K, indicating that they were due to excited-state transitions. The signal at $g = 5.15$ was nearly isotropic with a line width of less than 2.5 mT. An isotropic signal at $g = 5.15$ is not consistent with any of the $S = {}^1/_2$, ${}^3/_2$, or ${}^5/_2$ systems from TaFd detected in this work. It may be that these signals can be assigned to the first excited-state transition of an $S = {}^7/_2$ system ($E/D = 0.12$), and even an assignment to the first excited-state transition of an $S = {}^9/_2$ system ($E/D = 0.4$) cannot be excluded. However, the accompanying EPR signals expected for both assignments are missing, perhaps because of their low intensities or high line widths. Both the signals at $g = 5.15$ and 7.3 have a derivative form which does not fit with any of the assigned spin systems in TaFd. Excited-state transitions with $g = 7.3$ can only be observed from spin systems where $S > {}^5/_2$ (*16*). However, the spin concentration of both these excited-state EPR signals is very low (<1%) so that they make only a minor contribution to the magnetic properties of TaFd and they will be ignored in our subsequent analysis.

DISCUSSION

A ferredoxin from *T. aromatica* has very recently been purified and biochemically characterized. The data obtained in this work by cyclic voltammetry and multifrequency EPR indicate that it contains two [4Fe-4S] clusters with unusual properties: (i) they have different spin states, (ii) they interact magnetically, (iii) this interaction strongly depends on temperature, and (iv) they have widely differing reduction potentials.

The ferredoxin of *T. aromatica* is the third [4Fe-4S] ferredoxin of the CvFd type to be described in which the clusters have been shown to have considerably different reduction potentials. The other two examples, observed by cyclic voltammetric, EPR, and circular dichroism studies, are CvFd from *C. vinosum* and AvFdIII from *A. vinelandii* (*11*−*13*). It is evident that there must be a close relationship between their unusual cluster ligation and different electrochemical properties when CvFd-type ferredoxins are compared with CpFd-type ferredoxins (Table 1). The question arises whether it is in general possible to assign such unusual electrochemical properties of Fe−S clusters to an unusual ligation.

The three-dimensional structure of CvFd has been determined (*17*). Taken together with electrochemical data from molecular variants with modifications in the protein environment close to the individual cluster ligation sites (*11*), these data enabled the assignment of the two redox transitions to the individual clusters. It was surprising that the cluster with the unusual ligation (termed cluster II in CvFd) was the one with the reduction potential similar to those of typical CpFd types (ca. −400 mV; Table 1). The cluster with the unusual low reduction potential in CvFd-type ferredoxins is ligated by the first three cysteines of the typical Fe−S binding motif CXXCXXCXX*CP close to the N-terminus and by the last cysteine of the second more unusual motif close to the C-terminus (*9*) (Table 1). A bulky nonpolar residue at the X* position has been associated with this negative potential (e.g., valine in CvFd and AvFdIII). This fits to the data from TaFd, where valine is replaced with the less bulky alanine residue, perhaps resulting in an increase in the reduction potential of cluster B of ∼70 mV compared to that of CvFd or AvFdIII. However, the more intriguing feature of CvFd-type ferredoxins is the presence of two [4Fe-4S] clusters with very different formal reduction potentials.

EPR Spectroscopic Properties of the [4Fe-4S] Clusters of TaFd. The main aim of this work was to characterize the [4Fe-4S] clusters of TaFd by combining cyclic voltammetric with EPR spectroscopic techniques. The results from cyclic voltammetry have enabled us to assign EPR spectra poised at all potentials to the degree of reduction of each of the [4Fe-4S] clusters. The EPR spectrum of fully reduced TaFd is very similar to those of the *C. vinosum*-type ferredoxins, AvFdIII (*13*) and CvFd (*10*, *12*). Spectra of the fully reduced protein clearly indicate a magnetic interaction between the reduced clusters. Cluster A in TaFd is $S = {}^5/_2$ and couples with the other $S = {}^1/_2$ cluster, whereas in CvFd, both clusters are $S = {}^1/_2$. Thus, the characteristics of the cluster ligation motifs in CvFd-type ferredoxins determine the redox properties of the [4Fe-4S] clusters but not their spin states. It is

extremely difficult to make general statements about how the protein environment determines the magnetic and electrochemical properties of [4Fe-4S] clusters. It is probable that very small alterations in the amino acids in the vicinity of a cluster result in small distortions of the cluster geometry. In a [4Fe-4S] cluster, all four iron atoms are usually high-spin ($S = {}^5/_2$ or 2) and couple antiferromagnetically (*16*). As a consequence of cluster perturbation, this antiferromagnetic coupling could be affected, and this may result in a switch from low-spin to high-spin states for the cluster as a whole. Depending on the applied potential, TaFd displays EPR signals of $S = {}^3/_2$, ${}^5/_2$ (most probably cluster A), and ${}^7/_2$ and/or ${}^9/_2$ (not assigned to a cluster) high-spin systems. Since the voltammetry is fully consistent with a single A cluster species undergoing redox transitions, these spin states are unlikely to arise from sample heterogeneity. There are several examples of $S = {}^3/_2$ spin states of [4Fe-4S] clusters in proteins (*19*−*25*) and in synthetic $[Fe_4S_4(SR)_4]^{3-}$ analogues (*26*). To our knowledge, only two examples of $S = {}^5/_2$ spin states from biological [4Fe-4S] clusters have been described: glutamine phosphoribosylpyrophosphate amidotransferase from *Bacillus subtilis* (*27*) and nucleotide-bound iron protein of nitrogenase from *A. vinelandii* (*24*). In both cases, the occurrence of the $S = {}^5/_2$ state was accompanied by $S = {}^1/_2$ and ${}^3/_2$ spin states, and in the case of glutamine phosphoribosylpyrophosphate amidotransferase, the contribution of the $S = {}^5/_2$ state to the spin mixture even depended on the enzyme concentration. $S = {}^7/_2$ systems of [4Fe-4S] cluster-containing proteins have been detected in some, but not all, selenium-substituted clostridial-type ferredoxins (*25*) and in the benzoyl-CoA reductase from *T. aromatica* (*28*). In all cases, the high-spin signals were part of a spin mixture. This indicates that once the geometry of a [4Fe-4S] cluster is distorted relative to a conventional $S = {}^1/_2$ cluster, the composition of different spin states in a mixed-spin system is highly sensitive to minor alterations of the protein environment. Observations with TaFd support this assumption. First, in the redox titration experiments with cluster A, the ratio of the amplitude of the $S = {}^3/_2$ signal to that of the $S = {}^5/_2$ signal changed with the degree of reduction of the cluster, with the relative contribution of the $S = {}^3/_2$ state increasing with its degree of reduction (Figure 4). Second, although only the $S = {}^3/_2$ and ${}^5/_2$ high-spin signals were observed at potentials where only cluster A was reduced, the relative signal intensities varied slightly between different preparations. Third, at potentials where both clusters are reduced, signals at $g = 5.15$ and 7.3 were observed which can only be assigned to spin systems where $S > {}^5/_2$, indicating that the state of reduction of one cluster affects the spin state of the other. It is important to remember that these EPR measurements can only be made in frozen solutions and that it is possible that the spin states of different [4Fe-4S] clusters in proteins can show different sensitivities to the freezing procedure to give different spin-state mixtures as observed by EPR.

As had previously been shown for CvFd ferredoxin, the coupling between the [4Fe-4S] clusters in TaFd exhibited an unusual temperature dependence. Spectra at 20 K indicated single, isolated species, whereas at 4 K, EPR spectra clearly displayed signals resulting from magnetic interactions between clusters. In CvFd, this phenomenon was explained by different relaxation properties of both $S = {}^1/_2$ clusters (*12*). From the temperature dependence of its EPR signal, cluster I in CvFd, which has the more negative reduction potential, relaxes much faster than cluster II, and the suggestion was that therefore the magnetic interaction between the clusters can only be observed at low temperatures. This was confirmed by determining the spin concentrations, which at 4 K indicated two reduced clusters per molecule, and at 20 K showed less than one paramagnetic cluster per molecule. Our results with TaFd suggest that this phenomenon must have a different explanation because (i) in 80% reduced TaFd, the spin concentration of the split $S = {}^1/_2$ EPR signals indicated the presence of only one reduced cluster of this type; (ii) under nonsaturating conditions, its spin concentration was constant between 4 and 30 K; and (iii) the temperature-dependent switch from split to nonsplit EPR spectra was observed for the $S = {}^1/_2$ and ${}^5/_2$ signals in the same temperature range. This suggests that differences between the relaxation properties of the clusters are unlikely to be the reasons for the observed phenomenon in TaFd. It appears that the relaxation rates of both clusters need to be sufficiently slow for the interaction to be able to be observed by EPR, and that the coupling is seen, or not seen, in the spectrum of both clusters simultaneously. It is also evident that, at least in this case, since both EPR signals are observed above the temperature where their splitting disappears, the relaxation rate required to observe the interaction is slower than that needed to sharpen the EPR spectra fully.

ACKNOWLEDGMENT

We thank Drs. F. E. Mabbs and E. J. L. McInnes of the EPSRC c.w. EPR Service Centre at the University of Manchester (Manchester, U.K.) for Q- and S-band EPR spectra and Dr. S. J. George for many useful discussions.

REFERENCES

1. Heider, J., and Fuchs, G. (1997) *Eur. J. Biochem. 243*, 577−596.
2. Harwood, C. S., and Gibson, J. (1997) *J. Bacteriol. 179*, 301−309.
3. Tschech, A., and Fuchs, G. (1987) *Arch. Microbiol. 148*, 213−217.
4. Anders, H.-J., Kaetzke, A., Kämpfer, P., Ludwig, W., and Fuchs, G. (1995) *Int. J. Syst. Bacteriol. 45*, 327−333.
5. Boll, M., and Fuchs, G. (1995) *Eur. J. Biochem. 234*, 921−933.
6. Brackmann, R., and Fuchs, G. (1993) *Eur. J. Biochem. 213*, 563−571.
7. Breese, K., and Fuchs, G. (1998) *Eur. J. Biochem. 251*, 916−923.
8. Boll, M., and Fuchs, G. (1998) *Eur. J. Biochem. 251*, 946−954.
9. Moulis, J.-M. (1996) *Biochim. Biophys. Acta 1308*, 12−14.
10. Huber, J.-G., Gaillard, J., and Moulis, J.-M. (1995) *Biochemistry 34*, 194−205.
11. Kyritsis, P., Hatzfeld, O. M., Link, T. A., and Moulis, J. M. (1998) *J. Biol. Chem. 273*, 15404−15411.
12. Kyritsis, P., Kümmerle, R., Huber, J. G., Gaillard, B., Popescu, C., Münck, E., and Moulis, J.-M. (1999) *Biochemistry 38*, 6335−6345.
13. Gao-Sheridan, H. S., Pershad, H. R., Armstrong, F. A., and Burgess, B. K. (1998) *J. Biol. Chem. 273*, 5514−5519.
14. Bard, A. J., and Faulkner, L. R. (1980) in *Electrochemical Methods: Fundamentals and Applications*, Wiley, New York.
15. Armstrong, F. A., Butt, J. N., and Sucheta, A. (1993) *Methods Enzymol. 227*, 479−500.

16. Hagen, W. R. (1992) *Adv. Inorg. Chem. 38*, 165−222.
17. Moulis, J.-M., Sieker, L. C., Wilson, K. S., and Dauter, Z. (1996) *Protein Sci. 5*, 1765−1775.
18. Breton, J. L., Duff, J. L., Armstrong, F. A., George, S. J., Petillot, Y., Forest, E., Schafer, G., and Thomson, A. J. (1995) *Eur. J. Biochem. 233*, 937−946.
19. Hagen, W. R., Eady, R. R., Dunham, W. R., and Haaker, H. (1985) *FEBS Lett. 189*, 250−254.
20. George, S. J., Armstrong, F. A., Hatchikian, E. C., and Thomson, A. J. (1989) *Biochem. J. 264*, 275−284.
21. Conover, R. C., Kowal, A. T., Jae-Bum Park, W. F., Aono, S., Adams, M. W. W., and Johnson, M. K. (1990) *J. Biol. Chem. 265*, 8533−8541.
22. Duin, E. C., Lafferty, M. E., Crouse, B. R., Allen, R. M., Sanyal, I., Flint, D. E., and Johnson, M. K. (1997) *Biochemistry 36*, 11811−11820.
23. Arendsen, F. A., Hadden, J., Card, G., McAlpine, A. S., Bailey, S., Zaitsev, V., Duke, E. H. M., Lindley, P. F., Kröckel, M., Trautwein, A. X., Feiters, M. C., Charnock, J. M., Garner, C. D., Marritt, S. J., Thompson, A. J., Kooter, I. M., Johnson, M. K., van den Berg, W. A. M., van Dongen, W. M. A. M., and Hagen, W. R. (1998) *J. Biol. Inorg. Chem. 3*, 81−95.
24. Lindahl, P. A., Gorelick, N. J., Münck, E., and Orme-Johnson, W. H. (1987) *J. Biol. Chem. 262*, 14945−14953.
25. Gaillard, J., Moulis, J.-M., Auric, P., and Meyer, J. (1986) *Biochemistry 25*, 464−468.
26. Carney, M. J., Papaefthymiou, G. C., Spartalian, R. B., Frankel, R. B., and Holm, R. H. (1988) *J. Am. Chem. Soc. 110*, 6084−6095.
27. Oñate, Y. A., Vollmer, S. J., Switzer, R. L., and Johnson, M. K. (1989) *J. Biol. Chem. 264*, 18386−18391.
28. Boll, M., Albracht, S. J. P., and Fuchs, G. (1997) *Eur. J. Biochem. 244*, 840−851.

BI9927890